International Journal of Power Electronics and Drive Systems (IJPEDS)
Vol. 15, No. 2, June 2024, pp. 1017~1030
ISSN: 2088-8694, DOI: 10.11591/ijpeds.v15.i2.pp1017-1030

Analysis of the effect of mutual inductance on reducing output current ripple of the modified DC-DC Cuk converter

Nabil Driantama, Andriazis Dahono, Arwindra Rizqiawan, Jihad Furqani
School of Electrical Engineering and Informatics, Institut Teknologi Bandung, Bandung, Indonesia

Article Info

Article history:

Received Jun 21, 2023
Revised Nov 29, 2023
Accepted Dec 14, 2023

Keywords:

Cuk converter
DC-DC converter
Modified Cuk converter
Mutual inductance
Ripple

ABSTRACT

DC-DC converters exhibiting minimal input and output ripple are extensively employed across a diverse range of applications. This paper presents a proposed modification to the DC-DC Cuk converter. The converter is developed by modifying a conventional Cuk DC-DC converter to exhibit boost characteristics. The DC-DC converters possess the capability to function as versatile units that can be employed in a multitude of applications, ranging from DC-DC conversion to DC-AC conversion (inversion). This paper presents a novel DC-DC converter design that aims to achieve reduced ripple in both input and output currents. By employing the principle of mutual inductance, it is possible to further mitigate the presence of ripple current. The analysis of the impact of mutual inductance on the output voltage and ripple current of the proposed converter has been conducted. The validity of the derived analytical method has been confirmed through both simulated and experimental investigations. The utilization of mutual inductance in the proposed modified Cuk converter has been demonstrated to result in reduced current ripple.

Corresponding Author:

Arwindra Rizqiawan
School of Electrical and Informatics, Institut Teknologi Bandung
Ganesha 10, Lb. Siliwangi, Coblong, Bandung, West Java 40132, Indonesia
Email: windra@itb.ac.id

NOMENCLATURE

C	: Capacitor C	I_L	: Load current	T_{ON}	: On time Q switch
C_d	: Capacitor C_d	i_o	: Inductor current L_o	T_s	: Switching period
C_o	: Capacitor C_o	L_d	: Inductor L_d	V_{Q0}	: Switch voltage Q
R_Q	: Switch resistance	L_m	: Inductor L_m	V_c	: Capacitor voltage C
D_1, D_2	: Diode 1, 2	M	: Mutual inductance	V_D	: Diode drop voltage D
E_d	: Voltage source	L_o	: Inductor L_o	V_{D0}	: Diode voltage D
T_{OFF}	: Off time Q switch	Q1, Q2, Q3, Q4	: Upper and lower arm switch	V_L	: Load voltage
f_s	: Switching frequency	R_d, R_o	: Inductor resistance L_d and L_o	V_Q	: Switch drop voltage Q
I_C	: Capacitor current C	R_D	: Diode resistance	α	: Duty cycle
i_d	: Inductor current L_d	t, t_0, t_1, t_2, t_3, t_4	: Time period	Δ	: Tilde
i_D	: Diode current	t_{dead}	: Deadtime		

1. INTRODUCTION

The power converters are extensively utilized in a diverse range of applications, including high-voltage direct current (HVDC) transmission, flexible alternating current transmission systems (FACTS),

microgrids, generators based on renewable energy sources, AC motor control, and other related fields [1]–[3]. The power converter that is necessary can take the form of a DC-DC converter, a DC-AC inverter, an AC-DC rectifier, or an AC-AC converter. The DC-DC boost converter is presently the most frequently employed type of DC-DC converter. A power converter with a high voltage ratio is often necessary in various applications. Nevertheless, it is important to note that converters with a high ratio exhibit elevated levels of current ripples in practical applications [4]–[7]. The presence of significant fluctuations in current or voltage can have detrimental effects on the lifespan of equipment and can lead to excessive strain on components within power converters. Furthermore, it is worth noting that common mode ripple has been found to induce elevated levels of bearing currents in electric motors, as evidenced by previous studies [8]–[11].

In the context of a solar power plant, it has been observed that the presence of common mode ripple results in the generation of elevated levels of leakage currents [12], [13]. Hence, an effective converter should generate minimal differential mode ripple and exhibit minimal common mode ripple. Various methodologies and techniques have been employed by prior researchers in order to mitigate the presence of current ripple in power converters. Various techniques and methods employed in converters include enhancing the switching frequency and inductance, as well as utilizing interleaved and multiphase approaches [14]–[22]. The implementation of a multiphase or interleave converter has been shown to effectively mitigate the current ripple in the converter [23]–[25]. The reduction in current ripple in the multiphase converter is attributed to the varying switching phase angles across each converter phase, resulting in cancellation of input or output current ripple. Nevertheless, a notable drawback of the multiphase converter lies in its reliance on a substantial number of switches and intricate converter control mechanisms. The achievement of a significantly low current ripple is contingent upon the utilization of specific duty cycles for the switch. Consequently, this constraint imposes limitations on the converter's controlling capacity. Furthermore, it is worth noting that the voltage drop will be amplified due to the substantial voltage drop occurring at the switch.

The current ripple in a power converter can be influenced by four key factors: the switching frequency, the source voltage, the duty cycle, and the inductance value. The voltage source supplying the power converter lacks adjustability. By elevating the switching frequency, there will be a corresponding reduction in the magnitude of the ripple current that traverses the power converter. Nevertheless, the act of elevating the switching frequency leads to a corresponding increase in switching losses, there by causing a decline in overall efficiency. The switch exhibits a notable susceptibility to high stress conditions, thereby contributing to a heightened likelihood of failure. In addition to the afore mentioned considerations, it is worth noting that augmenting the inductance value can also serve as a means to mitigate current ripple. However, it is important to acknowledge that this particular approach necessitates an increase in both the physical dimensions and volume of the inductor. The acquisition of high-quality inductor cores is a costly endeavor, thereby resulting in an increase in the overall cost of the converter.

This study presents a proposal for the implementation of a mutual inductor in order to mitigate the output current ripple in a modified Cuk converter. The implementation of mutual inductance in the converter results in a reduction of current ripple. This reduction is achieved by increasing the overall effectiveness of inductance, without the necessity of augmenting the quantity or size of inductors. The utilization of mutual inductors enables the converter to operate with a single inductor core, while effectively emulating the behavior of two separate inductors. Consequently, this configuration reduces the number of components required in the converter. The addition of switches to the converter is unnecessary in order to minimize losses associated with components and switches. The minimization of voltage drop is achievable due to the converter's reliance on a limited number of components. This study aims to investigate the impact of mutual inductance in a power converter based on a modified Cuk converter [23]. The modified cuk converter exhibits a relatively low magnitude of current ripple. However, the implementation of mutual inductance allows for further reduction of the current ripple.

This paper is structured as follows: i) Section 1 provides an overview of the introduction and presents the problem that will be addressed; ii) Section 2, an analysis of the modified Cuk DC-DC converter is presented; iii) Section 3 of the report provides a comprehensive analysis of the ripple phenomenon observed in the modified Cuk DC-DC power converter, with particular emphasis on the influence of mutual inductance; iv) Section 4 of the report provides a comprehensive analysis of the voltage characteristics exhibited by the modified Cuk DC-DC power converter, with particular emphasis on the influence of mutual inductance; v) Section 5 provides a comprehensive account of the experimental findings pertaining to the utilization of mutualinductance in the modified Cuk DC-DC power converter. Furthermore, it critically assesses the outcomes obtained from the experimentation. Lastly, the concluding section, section 6, presents the findings and implications of our study.

2. MODIFIED DC-DC CUK CONVERTER

In 1977, Prof. Slobodan Cuk from the California Institute of Technology proposed another conventional converter known as the Cuk DC-DC power converter [15]. The converter is derived based on a combination of boost and buck converters or as a dual of the buck-boost converter. The proposed DC-DC power converter is a modification result of conventional Cuk DC-DC power converter. The basic scheme of Cuk DC-DC power converter is shown in Figure 1. Though the active switching device is shown using metal oxide semiconductor field effect transistor (MOSFET), other type switching device can also be used. Under continuous conduction mode, it can be shown that the voltage ratio is shown in (1).

$$\frac{\overline{v}_o}{E_d} = \frac{\alpha}{1-\alpha} \tag{1}$$

Where $\alpha=T_{ON}/T_s$ is the duty cycle of transistor Q, T_{ON} is ON-period of transistor Q, and T_s is the switching period. The converter has a capability to produce an output voltage that is lower or higher than the DC input voltage. The power converter has continuous input and output currents with the associated low ripple content. Unfortunately, the polarity of the DC output voltage is reversed.

As it is shown in Figure 1, there is a third terminal that a load can be connected. The voltage ratio of the third terminal is shown in (2), where $\overline{v}_L$ is the voltage differential of the third terminal.

$$\frac{\overline{v}_L}{E_d} = \frac{1}{1-\alpha} \tag{2}$$

If the load is connected to the third terminal, the load voltage is always higher than the input voltage. The voltage polarity of this third terminal is not reversed. For the same duty cycles, the voltage of third terminal is higher than the conventional load terminal. Fortunately, in our applications, the desired output voltage is always higher than the input voltage. If the load is connected to the third terminal, then a new power converter as shown in Figure 2 can be obtained. The load voltage is always higher than the input voltage as in the case of conventional boost DC-DC power converter. Different to the conventional one, however, the modified Cuk converter in Figure 2 has a continuous output current with the associated low ripple content. Further, the two inductors can be coupled in one core as shown in Figure 3 to utilize its mutual inductance.

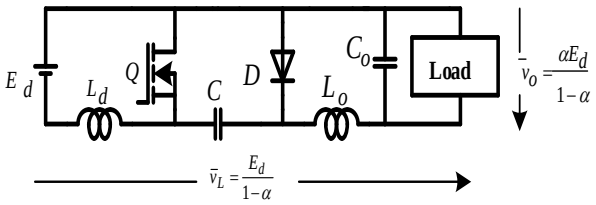

Figure 1. Modification of Cuk power converter

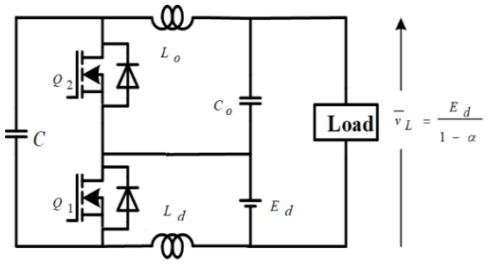

Figure 2. Modified Cuk power converter with self-inductance

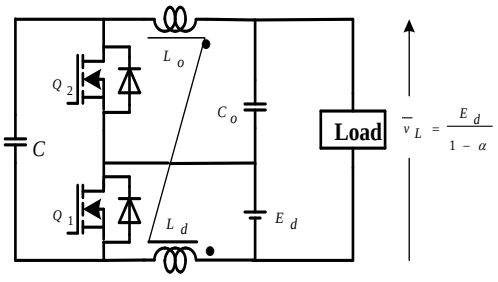

Figure 3. Modified Cuk power converter with mutual inductance

3. RIPPLE ANALYSIS

In this section, the analysis of ripple current in a modified DC-DC Cuk converter that uses self-inductance and mutual inductance is explained. The first thing to do in current ripple analysis is to determine

the state conditions (state 1 and state 2), followed by Kirchhoff's current law (KCL) and Kirchhoff's voltage law (KVL) analysis in each state condition. Afterwards, forming a state space average matrix and substituting current and voltage values into their ripple values. Then, separate the average value from the ripple value so that a current ripple state space matrix is formed and the state space results are used to obtain the current ripple value using the integral mathematical method. These results are substituted into the value of the current ripple equation in two conditions (ON/OFF switch) to get the current ripple value. The resulting ripple current value is substituted into the root mean square current ripple value to get the final result of the current ripple value in the converter. Figure 4, the mentioned analysis is illustrated in the flowchart. The flowchart shows the required analysis to determine the ripple value of the current produced in the converter.

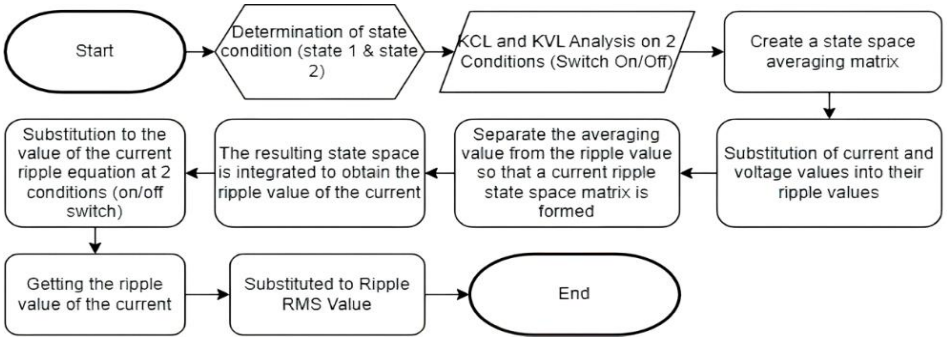

Figure 4. Flowchart of the analysis to determine the ripple value in the converter

Based on Figure 5, transistors Q1 and Q2 will always receive opposite command signals. When transistor Q1 receives an ON signal, transistor Q2 will receive an OFF signal, this also applies to the opposite condition. Figure 5(a) shows the current flow when transistor Q1 receives an ON signal while transistor Q2 receives an OFF signal, and Figure 5(b) shows the current when transistor Q1 receives an OFF signal while transistor Q2 receives an ON signal.

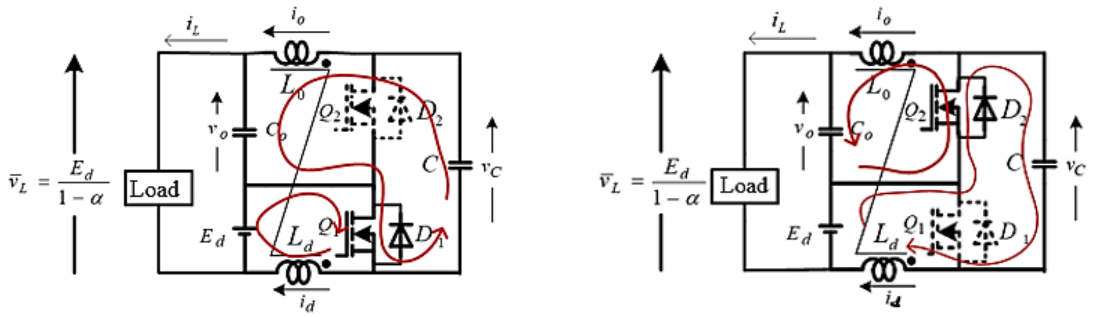

Figure 5. Converter condition when transistor Q receives an (a) ON-signal and (b) OFF-signal

In the following analysis, it is assumed that all transistors are ideal, and the inductor resistance is neglected. Input voltage and load current are assumed to be pure DC voltage and constant current without ripple. Based on Figure 5, the following can be obtained as shown in (3).

$$\begin{bmatrix} L_d & M \\ M & L_o \end{bmatrix} \begin{bmatrix} \frac{di_d}{dt} \\ \frac{di_o}{dt} \end{bmatrix} = \begin{bmatrix} E_d - v_{Q1} \\ v_{Q2} - v_o \end{bmatrix} \quad (3)$$

Where V_Q and V_D are voltages across transistor *Q* dan diode *D*, respectively, and *M* is the mutual inductance between L_d and L_o. The currents and voltages can be divided into the average and ripple components as in the (4)-(8).

$$i_d = I_d + \tilde{\imath}_d \tag{4}$$

$$i_o = I_o + \tilde{\imath}_o \tag{5}$$

$$v_{Q1} = V_{Q1} + \tilde{v}_{Q1} \tag{6}$$

$$v_{Q2} = V_{Q2} + \tilde{v}_{Q2} \tag{7}$$

$$v_o = V_o + \tilde{v}_o \tag{8}$$

Where tilde and bar indicate ripple and average components, respectively. If (4)-(8) are substituted into (3) then the current ripple components can be obtained as in (9).

$$\begin{bmatrix} L_d & M \\ M & L_o \end{bmatrix} \begin{bmatrix} \frac{d\tilde{\imath}_d}{dt} \\ \frac{d\tilde{\imath}_o}{dt} \end{bmatrix} = \begin{bmatrix} -\tilde{v}_{Q1} \\ \tilde{v}_{Q2} - \tilde{v}_o \end{bmatrix} \tag{9}$$

Based on (9), we get the following ripple current as in (10) and (11).

$$\tilde{\imath}_d = \frac{L_o}{\Delta}\int\left(-\tilde{v}_{Q1}\right)dt - \frac{M}{\Delta}\int\left(\tilde{v}_{Q2} - \tilde{v}_o\right)dt + C_1 \tag{10}$$

$$\tilde{\imath}_o = \frac{L_d}{\Delta}\int\left(\tilde{v}_{Q2} - \tilde{v}_o\right)dt - \frac{M}{\Delta}\int\left(-\tilde{v}_{Q1}\right)dt + C_2 \tag{11}$$

Where Δ is the determinant of the inductance matrix of (9) and C_1 and C_2 are the integration constants, the voltage ripple on the switch is much higher than the ripple on the capacitor, we can assume as in (12).

$$\tilde{v}_{Q2} >> \tilde{v}_o \tag{12}$$

So, (10) and (11) can be approximated by (13) and (14).

$$\tilde{\imath}_d = \frac{L_o}{\Delta}\int\left(-\tilde{v}_{Q1}\right)dt - \frac{M}{\Delta}\int \tilde{v}_{Q2}dt + C_1 \tag{13}$$

$$\tilde{\imath}_o = \frac{L_d}{\Delta}\int \tilde{v}_{Q2}dt - \frac{M}{\Delta}\int\left(-\tilde{v}_{Q1}\right)dt + C_2 \tag{14}$$

Based on (6) and (7), the switch voltage ripple can be derived as in (15) and (16).

$$\tilde{v}_{Q1} = v_{Q1} - V_{Q1} \tag{15}$$

$$\tilde{v}_{Q2} = v_{Q2} - V_{Q2} \tag{16}$$

In which some assumptions can be derived as in (17) and (18), related to (15) and (16).

$$V_{Q1} = E_d \tag{17}$$

$$V_{Q2} = V_o = \frac{\alpha}{1-\alpha}E_d \tag{18}$$

When switch Q1 receives an ON signal and switch Q2 receives an OFF signal, the voltages of switches Q1 and Q2 are shown in (19) and (20).

$$v_{Q1} = 0 \tag{19}$$

$$v_{Q2} = \tilde{v}_C = \frac{E_d}{1-\alpha} \tag{20}$$

Therefore, the ripple equations when switch Q1 receives the ON signal are shown in (21) and (22).

$$\tilde{\imath}_d = \frac{L_o - M}{\Delta} \int E_d dt + C_1 \tag{21}$$

$$\tilde{\imath}_o = \frac{L_d - M}{\Delta} \int E_d dt + C_2 \tag{22}$$

When switch Q2 receives the ON signal, the voltages of switches Q1 and Q2 are shown in (23) and (24).

$$v_{Q1} = \tilde{v}_C = \frac{E_d}{1-\alpha} \tag{23}$$

$$v_{Q2} = 0 \tag{24}$$

Therefore, the current ripple when transistor Q2 receives an ON signal is shown in (25) and (26).

$$\tilde{\imath}_d = -\frac{L_o - M}{\Delta} \int \frac{\alpha E_d}{1-\alpha} dt + C_3 \tag{25}$$

$$\tilde{i}_o = -\frac{L_d - M}{\Delta} \int \frac{\alpha E_d}{1-\alpha} dt + C_4 \tag{26}$$

Where, C_3 and C_4 are integration constants. Based on the above analysis, the current ripple expression in one switching period can be written as (27) and (28).

$$\tilde{\imath}_d = \frac{L_o - M}{\Delta} E_d \begin{cases} -\frac{T_{ON}}{2} + (t - t_o) & \text{For} \quad t_o \le t \le t_2 \\ \frac{\alpha}{1-\alpha}\frac{T_{OFF}}{2} - \frac{\alpha}{1-\alpha}(t - t_2) & \text{For} \quad t_2 \le t \le t_4 \end{cases} \tag{27}$$

$$\tilde{\imath}_o = \frac{L_d - M}{\Delta} E_d \begin{cases} -\frac{T_{ON}}{2} + (t - t_o) & \text{For} \quad t_o \le t \le t_2 \\ \frac{\alpha}{1-\alpha}\frac{T_{OFF}}{2} - \frac{\alpha}{1-\alpha}(t - t_2) & \text{For} \quad t_2 \le t \le t_4 \end{cases} \tag{28}$$

Figure 6 shows the current ripple wave during one switching period.

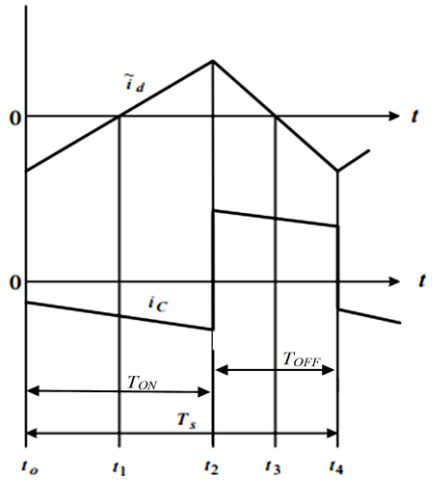

Figure 6. Converter current ripples over one carrier period

The rms value of current ripple during one switching period can be calculated in as in (29) and (30).

$$\tilde{I}_d = \left[\frac{1}{T_s}\int_{t_o}^{t_o+T_s} \tilde{\imath}_d^2 dt\right]^{1/2} \tag{29}$$

$$\tilde{I}_o = \left[\frac{1}{T_s}\int_{t_o}^{t_o+T_s} \tilde{\imath}_o^2 dt\right]^{1/2} \tag{30}$$

If we substitute (27) and (28) into (29) and (30) respectively, we get the current ripple expressions as shown in (31) and (32).

$$\tilde{I}_d = \frac{L_o - M}{2\sqrt{3}\Delta} \frac{\alpha E_d}{f_s} \tag{31}$$

$$\tilde{I}_o = \frac{L_d - M}{2\sqrt{3}\Delta} \frac{\alpha E_d}{f_s} \tag{32}$$

If the inductance L_d=L_o=L then (31) and (32) can be simplified into (33).

$$\tilde{I}_d = \tilde{I}_o = \frac{\alpha E_d}{2\sqrt{3} f_s (L+M)} \tag{33}$$

The (33) shows that the mutual inductance is proven to be able to increase the value of the effectiveness of inductance if it utilizes its mutual value. The current ripple will decrease because of the higher total effective inductance value due to mutual inductance.

4. VOLTAGE ANALYSIS

In conducting a voltage analysis, as in conducting previous ripple current analysis there are also steps that need to be done in order to obtain the appropriate results, these steps is illustrated in the flowchart shown in Figure 7. The first thing to do in the voltage analysis of the converter is to determine the state conditions (state 1 and state 2), followed by KCL and KVL analysis in each condition and form a state space averaging matrix. Then, determine the average values of associated voltages and currents. After that, we obtain the output voltage value which is assumed to have mutual inductance.

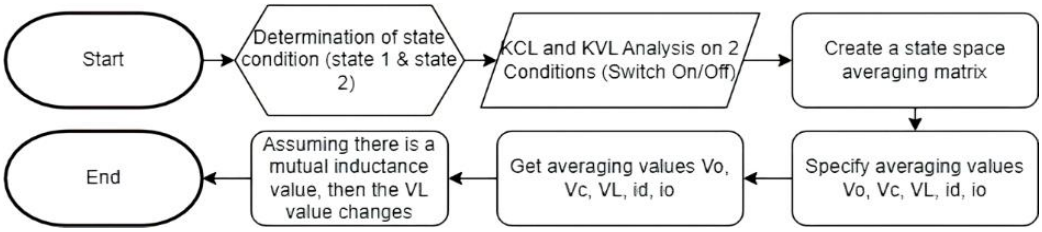

Figure 7. Flowchart analysis to determine the voltage value in the converter

Based on Figure 5, transistors Q1 and Q2 will always receive opposite command signals. When transistor Q1 receives an ON signal, transistor Q2 will receive an OFF signal, this also applies to the opposite condition. Figure 5(a) shows the current flow when transistor Q1 receives an ON signal while transistor Q2 receives an OFF signal, and Figure 5(b) shows the current when transistor Q1 receives an OFF signal while transistor Q2 receives an ON signal. Assuming the load current is positive, in this condition the current in the L_d and L_o inductors will increase. In order to make it more general, it is assumed that the voltage drops across the transistor and diode during conduction are (34) and (35).

$$v_Q = V_Q + R_Q i_Q \tag{34}$$

$$v_D = V_D + R_D i_D \tag{35}$$

Where V_Q and V_D are the constant components, and R_Q are R_D are the resistive components of voltage drops and i_Q and i_D are currents of transistor and diode, respectively. The resistances of the inductors L_d and L_o are R_d and R_o, respectively. Capacitors C and C_o are assumed as ideal capacitors with no inductance nor resistance. The capacitor equivalent series resistances can be neglected in this analysis as the average value of capacitor current is zero during steady-state, as shown in (36) and (37).

$$\begin{bmatrix} L_d & M \\ M & L_0 \end{bmatrix} \begin{bmatrix} \frac{di_d}{dt} \\ \frac{di_o}{dt} \end{bmatrix} = \begin{bmatrix} -(R_d + R_Q) & -R_Q \\ -R_Q & -(R_0 + R_Q) \end{bmatrix} \begin{bmatrix} i_d \\ i_0 \end{bmatrix} + \begin{bmatrix} E_d - V_{Q0} \\ V_C - V_0 - V_{Q0} \end{bmatrix} \tag{36}$$

$$\begin{bmatrix}\frac{di_d}{dt}\\ \frac{di_0}{dt}\end{bmatrix}=\begin{bmatrix}\frac{L_0}{\Delta} & -\frac{M}{\Delta}\\ -\frac{M}{\Delta} & \frac{L_d}{\Delta}\end{bmatrix}\begin{bmatrix}-(R_d+R_Q) & -R_Q\\ -R_Q & -(R_0+R_Q)\end{bmatrix}\begin{bmatrix}i_d\\ i_0\end{bmatrix}+\begin{bmatrix}\frac{L_0}{\Delta} & -\frac{M}{\Delta}\\ -\frac{M}{\Delta} & \frac{L_d}{\Delta}\end{bmatrix}\begin{bmatrix}E_d-v_{Q0}\\ v_C-v_0-v_{Q0}\end{bmatrix} \quad (37)$$

In the same way, we can get the equation when Q2 receives an ON signal. In this condition transistor Q2 that receives the ON signal, then we get the expression as in (38) and (39).

$$\begin{bmatrix}L_d & M\\ M & L_0\end{bmatrix}\begin{bmatrix}\frac{di_d}{dt}\\ \frac{di_o}{dt}\end{bmatrix}=\begin{bmatrix}-(R_d+R_D) & -R_D\\ -R_D & -(R_0+R_D)\end{bmatrix}\begin{bmatrix}i_d\\ i_0\end{bmatrix}+\begin{bmatrix}E_d-v_{D0}-v_C\\ -v_0-v_{D0}\end{bmatrix} \quad (38)$$

$$\begin{bmatrix}\frac{di_d}{dt}\\ \frac{di_0}{dt}\\ \frac{dv_C}{dt}\\ \frac{dv_0}{dt}\end{bmatrix}=\begin{bmatrix}-\frac{L_0(R_d+R_D)}{\Delta}+\frac{MR_D}{\Delta} & -\frac{L_0R_D}{\Delta}+\frac{M(R_0+R_D)}{\Delta} & -\frac{L_0}{\Delta} & \frac{M}{\Delta}\\ -\frac{L_dR_D}{\Delta}+\frac{M(R_d+R_D)}{\Delta} & -\frac{L_d(R_0+R_D)}{\Delta}+\frac{MR_D}{\Delta} & \frac{M}{\Delta} & -\frac{L_d}{\Delta}\\ \frac{1}{C} & 0 & 0 & 0\\ 0 & \frac{1}{C_0} & 0 & 0\end{bmatrix}\begin{bmatrix}i_d\\ i_0\\ v_C\\ v_0\end{bmatrix}+\begin{bmatrix}\frac{L_0}{\Delta}(E_d-v_{D0})+\frac{M}{\Delta}v_{D0}\\ -\frac{M}{\Delta}(E_d-v_{D0})-\frac{L_d}{\Delta}v_{D0}\\ 0\\ -\frac{I_L}{C_0}\end{bmatrix} \quad (39)$$

Transistor Q1 receives an ON signal during α period while an OFF signal is received during (1-α) period. The average state space equation is obtained by averaging in (37) and (39), then the following steady-state expression is obtained as in (40).

$$0=\begin{bmatrix}-\frac{L_0[R_d+\alpha R_Q+(1-\alpha)R_D]-M[R_Q\alpha+R_D(1-\alpha)]}{\Delta} & -\frac{L_0[R_Q\alpha+R_D(1-\alpha)]-M[R_o+R_Q\alpha(1-\alpha)]}{\Delta} & -\frac{M\alpha+L_0(1-\alpha)}{\Delta} & \frac{M}{\Delta}\\ -\frac{L_d[R_Q\alpha+R_D(1-\alpha)]-M[R_d+R_Q\alpha+R_D(1-\alpha)]}{\Delta} & -\frac{L_d[R_0+R_Q\alpha+R_D(1-\alpha)]-M[R_Q\alpha+R_D(1-\alpha)]}{\Delta} & -\frac{L_d\alpha+M(1-\alpha)}{\Delta} & -\frac{L_d}{\Delta}\\ \frac{1-\alpha}{C} & -\frac{\alpha}{C} & 0 & 0\\ 0 & \frac{1}{C_0} & 0 & 0\end{bmatrix}\begin{bmatrix}\bar{i}_d\\ \bar{i}_0\\ \bar{v}_C\\ \bar{v}_0\end{bmatrix}+\begin{bmatrix}\frac{L_0[E_d-V_{Q0}\alpha-V_{D0}(1-\alpha)]+M[V_{Q0}\alpha+V_{D0}(1-\alpha)]}{\Delta}\\ -\frac{M[E_d-V_{Q0}\alpha-V_{D0}(1-\alpha)]+L_d[V_{Q0}\alpha+V_{D0}(1-\alpha)]}{\Delta}\\ 0\\ -\frac{I_L}{C_0}\end{bmatrix} \quad (40)$$

Based on (40), if it is assumed that $L_d = L_0$, $R_d = R_0$, and $M = 0$, we can obtain the following expressions as shown in (41)-(44).

$$\bar{i}_0 = I_L \quad (41)$$

$$\bar{i}_d = \frac{\alpha}{1-\alpha}\bar{i}_0 = \frac{\alpha}{1-\alpha}I_L \quad (42)$$

$$-L_dR_Q\frac{\alpha}{1-\alpha}I_L - L_d(R_d+R_Q)I_L + L_d\alpha\bar{v}_C - L_d\bar{v}_0 - L_dV_{Q0} = 0 \quad (43)$$

$$-L_d(R_d+R_Q)\frac{\alpha}{1-\alpha}I_L - L_dR_QI_L - L_d(1-\alpha)\bar{v}_C + L_d[E_d-V_{Q0}] = 0 \quad (44)$$

Based on (44), then capacitor voltage can be expressed as in (45).

$$\bar{v}_C = \frac{E_d-V_{Q0}}{1-\alpha} - \frac{R_d\alpha+R_Q}{(1-\alpha)^2}I_L \quad (45)$$

From (43) and (45), then the capacitor voltage v_o dan be expressed as in (46).

$$\bar{v}_o = \frac{\alpha E_d}{1-\alpha} - \frac{V_{Qo}}{1-\alpha} - \frac{R_d(1-2\alpha+2\alpha^2)+R_Q}{(1-\alpha)^2} I_L \quad (46)$$

The load voltage is obtained as in (47).

$$\bar{v}_L = E_d + \bar{v}_o = \frac{E_d - V_{Qo}}{1-\alpha} - \frac{R_d(1-2\alpha+2\alpha^2)+R_Q}{(1-\alpha)^2} I_L \quad (47)$$

If in the (47), it is assumed that there is mutual inductance exists, then the converter output voltage becomes (48).

$$\bar{v}_L = \frac{E_d - VQ_o}{1+M\alpha-\alpha} - \frac{R_d(1+2\alpha-2\alpha^2)+R_q}{(1+M\alpha-\alpha)(1-\alpha)} I_L + \frac{MR_d(1+2\alpha-2\alpha^2)+MR_q}{(1+M\alpha-\alpha)(1-\alpha)} I_L \quad (48)$$

In (46), it is the output voltage expression of conventional Cuk DC-DC power converter, while in (47) and (48) is the modified Cuk DC-DC power converter, in the case of self-inductance and mutual inductance, respectively. It can be seen that from (48), the value of the output voltage in the case of mutual inductance exists has no effect on the voltage drop compared to that using self-inductance. So, the use of mutual inductance has no effect on the performance of the converter, in this case is the voltage drop.

5. EXPERIMENTAL RESULTS

To ensure the validity of the analysis, simulations and experiments were performed on the proposed converter. The experimental procedure was carried out using the converter illustrated in Figures 2 and 3. The semiconductor utilized in this investigation is the IRFP460 metal-oxide-semiconductor field-effect transistor (MOSFET) model, characterized by an internal resistance of 0.042 ohm. The electrolytic capacitors employed in this investigation are designated as C and Co, and possess an equivalent capacitance of 470 uF. The experimental configuration employs a direct current (DC) input voltage of 36 volts. The comprehensive specifications of this test are outlined in Table 1.

Table 1. Parameters on modified DC-DC Cuk converter

Component	Value
Capacitor *C*	470 uF
Capacitor C_o	470 µF
Switching frequency	10 kHz
Inductor L_d dan L_o	2.05 mH
Mutual value *M*	2.05 mH dan 1.2 mH
Switch	MOSFET IRF460N
Deadtime	2 us

To examine the influence of self-inductance and mutual inductance on the modified Cuk DC-DC converter, this experimental investigation utilizes three separate inductors, as illustrated in Figure 8. The experimental procedure involves the utilization of two inductors with different cores to measure the self-inductance value. The inductors are arranged at a specific separation from one another, as illustrated in Figure 8(a). To attain a collective value that efficiently mitigates the existing ripple, inductors possess the choice of interconnecting or consolidating themselves within a shared core, as illustrated in Figure 8(b). Alternatively, this objective can also be achieved by utilizing two separate inductors that are interconnected within a solitary wire, as depicted in Figure 8(c).

The determination of the mutual inductance values is based on the simple experiment as shown in Figure 9. Based on Figure 9, the voltage expressions can be shown in (49)-(52).

$$v_1 = L_1 \frac{di}{dt} + M_{12} \frac{di}{dt} \quad (49)$$

$$v_2 = L_2 \frac{di}{dt} + M_{21} \frac{di}{dt} \quad (50)$$

$$v = v_1 + v_2 = L_1 \frac{di}{dt} + M_{12} \frac{di}{dt} + L_2 \frac{di}{dt} + M_{21} \frac{di}{dt} \quad (51)$$

$$v = (L_1 + L_2 + M_{12} + M_{21}) \frac{di}{dt} \quad (52)$$

By using the assumption that the mutual inductances are equal, as in (53).

$$M_{12} = M_{21} = M \tag{53}$$

Then, the voltage and equivalent inductance can be calculated as in (54) and (55).

$$v = (L_1 + L_2 + 2M)\ \frac{di}{dt} \tag{54}$$

$$L_{eq} = L_1 + L_2 + 2M \tag{55}$$

So, the mutual inductance value will be obtained, as shown in (56).

$$M = \frac{L_{eq} - L_1 - L_2}{2} \tag{56}$$

(a) (b) (c)

Figure 8. Inductors used in testing the modified Cuk DC-DC converter: (a) 2.05 mH self-inductance, (b) 2.05 mH mutual inductance, and (c) 1.2 mH mutual inductance

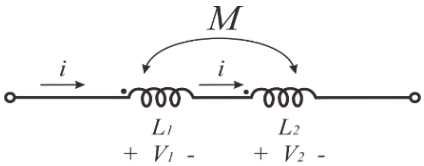

Figure 9. Mutual inductance values determination test

Mutual inductance value can be obtained by measuring the equivalent inductance value and its own inductance in inductors that have a mutual effect. Table 2 shows the differences in each inductance value, the measurement method used and the inductor model used in the test. The provision for obtaining a mutual value is that the mutual inductance value is not greater than the root of the sum of the two inductance values themselves as shown in (57).

$$M \leq \sqrt{L_1 + L_2} \tag{57}$$

Figure 10 shows an illustration of the equipment used in preparation for testing the power converter. The input side of the converter uses an AC source, transformer, LC filter and rectifier. Then, the converter gets a command signal from the microcontroller which generates the gate driver driving the converter. The output of the converter will have a resistive load of 200 ohms. Measurement equipment is needed to obtain the current ripple and voltage drop in the converter. The power meter is used to observe the value of the voltage drop in the converter, while to get the current ripple value, a current probe connected to an oscilloscope is used.

Measurement of inductor current ripple was carried out at a switching frequency of 10 kHz. This measurement was also carried out with various duty cycle values ranging from 0.1 to 0.8. To get the current waveform of the L_d and L_o inductors and their mutual inductance, a current probe is used which is mounted on the side of the inductor so that it can read the current that is passing through. Figure 11 shows the current waveform of self-inductance and mutual inductance at a duty cycle of 0.5. Figure 11(a) shows the current ripple waveform using mutual inductance value 0 mH, Figure 11(b) shows the current ripple waveform using mutual

inductance 1.2 mH, and Figure 11(c) shows the current ripple waveform using mutual inductance 2.05 mH. It can be seen that the inductor current waveform is continuous with small ripples. The ripple is reduced as the increment of the mutual inductance values. These waveforms confirm that the utilization of mutual inductance successfully reduces the current ripple of the modified Cuk converter.

Figure 12 shows a comparison of the calculation results of inductor ripple currents with mutual inductance and self-inductance measurement results. This figure clearly shows the accuracy of the proposed analytical method. The difference in the results of calculations and experiments is due to the voltage drop in the inductor resistance which is ignored in the calculations. These results confirm that the mutual inductance successfully reduces the current ripple in various duty cycle. Figure 13 shows the results of measuring the output voltage against the duty cycle. Experiments were carried out with variations in duty cycle from 0.1 to 0.8. The experiment was carried out with a constant load current. The blue curve shows the results of calculating the output voltage under ideal conditions (ignoring the resistance of the transistor and inductor). While the other curve is a curve that shows the results of calculating the output voltage under non-ideal conditions (by providing the resistance values of transistors, inductors and mutual values in converters that use mutual inductance). The experimental results are indicated by crosses, squares and triangles, where the experiments were carried out at a switching frequency of 10 kHz. From these results it can be seen that the experimental results are close to the calculation results. These results confirm that the utilization of mutual inductance does not deteriorate the performance of the converter, but still produces lower current ripple.

Table 2. The differences in inductance values, measurement methods and inductor models on converters

No	Mutual inductance (mH)	L_1 (mH)	L_2 (mH)	L_{eq} (mH)	Inductor model	Measurement method	Calculation	Figure
1	M=0	2.05	2.05	0	Two different cores and given the distance	Measured on each inductor	$M = \frac{0 - 2.05 - 2.05}{2}$ $M = \frac{0}{2} = 0\ mH$	
2	M=2.05	2.06	2.06	8.22	Coupled in the same cores	Using the dot to determine the polarity and get the L_{eq} value as well as the self-inductance value	$M = \frac{8.22 - 2.06 - 2.06}{2}$ $M = \frac{4.1}{2} = 2.05\ mH$	
3	M=1.2	1.4	1.4	5.2	Coupled in the same coil on 2 different cores	Using the dot to determine the polarity and get the L_{eq} value as well as the self-inductance value	$M = \frac{5.2 - 1.4 - 1.4}{2}$ $M = \frac{2.4}{2} = 1.2\ mH$	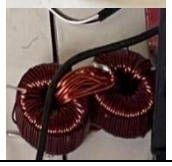

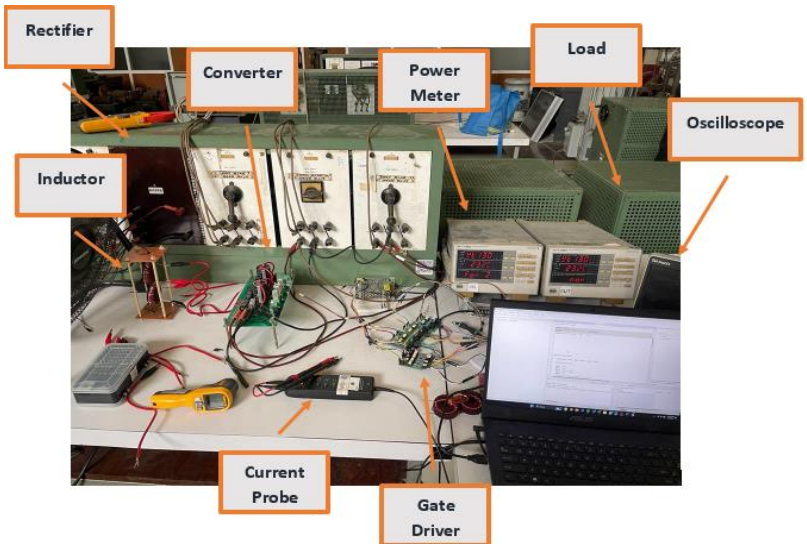

Figure 10. Laboratory experimental setup

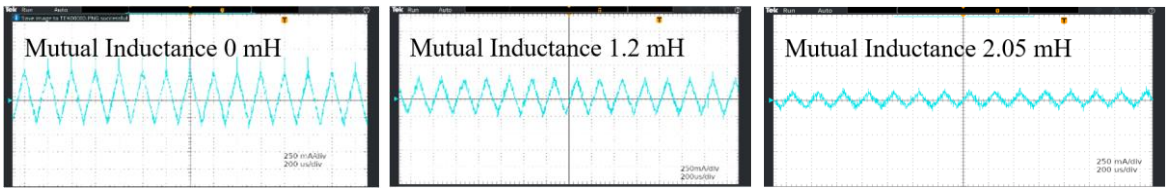

Figure 11. Current ripple waveform at 0.5 duty cycle with (a) self-inductance, (b) 1.2 mH mutual inductance, and (c) 2.05 mH mutual inductance

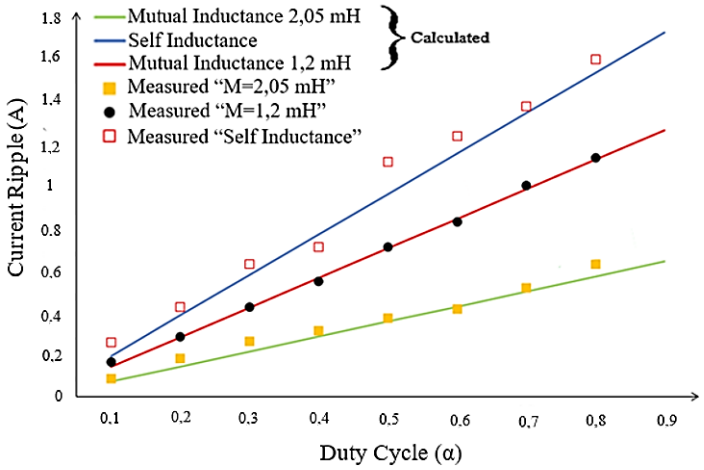

Figure 12. Comparation of experimental results inductor current ripple with self-inductance and mutual inductance of modified Cuk DC-DC power converter

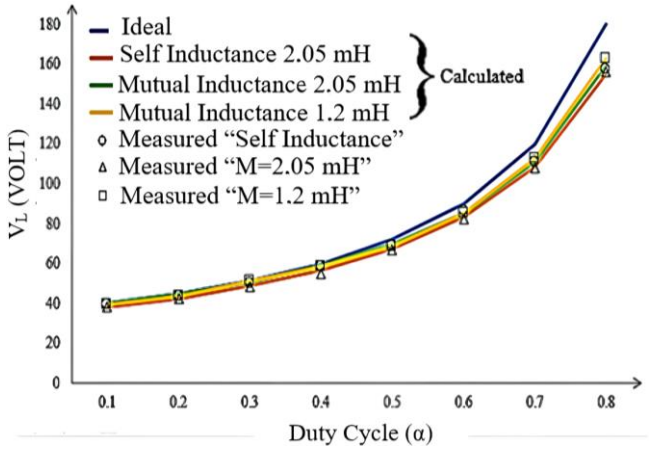

Figure 13. Comparison of experimental results and calculation of the output voltage on each inductor as a function of duty cycle of modified Cuk DC-DC power converter

6. CONCLUSION

The findings of this study indicate that the application of mutual inductance effectively mitigates current ripple in the modified DC-DC Cuk converter. The utilization of mutual inductance does not exert a substantial influence on the voltage drop, rendering it suitable for implementation in power electronics applications. The self-inductance and mutual inductance components of this converter have been subjected to testing, and the experimental findings indicate that they align with the analysis and calculations.

REFERENCES

[1] S. Bacha, D. Picault, B. Burger, I. Etxeberria-Otadui, and J. Martins, "Photovoltaics in microgrids: An overview of grid integration and energy management aspects," *IEEE Industrial Electronics Magazine*, vol. 9, no. 1, pp. 33–46, 2015, doi: 10.1109/MIE.2014.2366499.

[2] S. Kouro, J. I. Leon, D. Vinnikov, and L. G. Franquelo, "Grid-connected photovoltaic systems: An overview of recent research and emerging PV converter technology," *IEEE Industrial Electronics Magazine*, vol. 9, no. 1, pp. 47–61, 2015, doi: 10.1109/MIE.2014.2376976.

[3] P. A. Dahono, "New step-Up DC-DC converters for PV power generation systems," *2017 International Seminar on Intelligent Technology and Its Application: Strengthening the Link Between University Research and Industry to Support ASEAN Energy Sector, ISITIA 2017 - Proceeding*, vol. 2017-January, pp. 187–192, 2017, doi: 10.1109/ISITIA.2017.8124078.

[4] C. A. Ramos-Paja, D. González-Motoya, J. P. Villegas-Ceballos, S. I. Serna-Garcés, and R. Giral, "Sliding-mode controller for a photovoltaic system based on a Ćuk converter," *International Journal of Electrical and Computer Engineering*, vol. 11, no. 3, pp. 2027–2044, 2021, doi: 10.11591/ijece.v11i3.pp2027-2044.

[5] Ankit, S. K. Sahoo, S. Sukchai, and F. F. Yanine, "Review and comparative study of single-stage inverters for a PV system," *Renewable and Sustainable Energy Reviews*, vol. 91, pp. 962–986, 2018, doi: 10.1016/j.rser.2018.04.063.

[6] J. D. Paez, D. Frey, J. Maneiro, S. Bacha, and P. Dworakowski, "Overview of DC-DC Converters Dedicated to HVdc Grids," *IEEE Transactions on Power Delivery*, vol. 34, no. 1, pp. 119–128, 2019, doi: 10.1109/TPWRD.2018.2846408.

[7] B. T. Kadhem, S. S. Harden, and K. M. Abdulhassan, "High-performance Cuk converter with turn-on switching at zero voltage and zero current," *Bulletin of Electrical Engineering and Informatics*, vol. 12, no. 3, pp. 1359–1370, 2023, doi: 10.11591/eei.v12i3.4499.

[8] H. Akagi and S. Tamura, "A passive EMI filter for eliminating both bearing current and ground leakage current from an inverter-driven motor," *IEEE Transactions on Power Electronics*, vol. 21, no. 5, pp. 1459–1468, 2006, doi: 10.1109/TPEL.2006.880239.

[9] R. M. Tallam, G. L. Skibinski, T. A. Shudarek, and R. A. Lukaszewski, "Integrated differential-mode and common-mode filter to mitigate the effects of long motor leads on AC drives," *IEEE Transactions on Industry Applications*, vol. 47, no. 5, pp. 2075–2083, 2011, doi: 10.1109/TIA.2011.2161431.

[10] T. Sutikno, H. S. Purnama, R. A. Aprilianto, A. Jusoh, N. S. Widodo, and B. Santosa, "Modernisation of DC-DC converter topologies for solar energy harvesting applications: A review," *Indonesian Journal of Electrical Engineering and Computer Science*, vol. 28, no. 3, pp. 1845–1872, 2022, doi: 10.11591/ijeecs.v28.i3.pp1845-1872.

[11] A. Von Jouanne and P. N. Enjeti, "Design considerations for an inverter output filter to mitigate the effects of long motor leads in ASD applications," *IEEE Transactions on Industry Applications*, vol. 33, no. 5, pp. 1138–1145, 1997, doi: 10.1109/28.633789.

[12] S. S. Saswat, S. Patra, D. P. Mishra, S. R. Salkuti, and R. N. Senapati, "Harnessing wind and solar PV system to build hybrid power system," *International Journal of Power Electronics and Drive Systems*, vol. 12, no. 4, pp. 2160–2168, 2021, doi: 10.11591/ijpeds.v12.i4.pp2160-2168.

[13] D. Liu, H. Zhu, and R. Zhao, "Novel common-mode current suppression method in transformerless PV grid-connected system," *Applied Sciences (Switzerland)*, vol. 8, no. 11, 2018, doi: 10.3390/app8112072.

[14] C. V. Nguyen, H. Cha, D. Bui, and B. Choi, "Modified Double-Dual-Boost High-Conversion-Ratio DC-DC Converter With Common Ground and Low-Side Gate Driving," *IEEE Transactions on Power Electronics*, vol. 37, no. 5, pp. 4952–4956, 2022, doi: 10.1109/TPEL.2021.3130911.

[15] S. Ćuk and R. D. Middlebrook, "A new optimum topology switching DC-to-DC converter," *PESC Record - IEEE Annual Power Electronics Specialists Conference*, vol. 2015-March, pp. 160–179, 2015, doi: 10.1109/PESC.1977.7070814.

[16] C. T. Pan and C. M. Lai, "A high-efficiency high step-up converter with low switch voltage stress for fuel-cell system applications," *IEEE Transactions on Industrial Electronics*, vol. 57, no. 6, pp. 1998–2006, 2010, doi: 10.1109/TIE.2009.2024100.

[17] Q. Li *et al.*, "An Improved Floating Interleaved Boost Converter with the Zero-Ripple Input Current for Fuel Cell Applications," *IEEE Transactions on Energy Conversion*, vol. 34, no. 4, pp. 2168–2179, 2019, doi: 10.1109/TEC.2019.2936416.

[18] K. D. Joseph, A. E. Daniel, and A. Unnikrishnan, "Interleaved Cuk Converter with reduced switch current," *Proceedings of 2018 IEEE International Conference on Power, Instrumentation, Control and Computing, PICC 2018*, pp. 1–6, 2018, doi: 10.1109/PICC.2018.8384803.

[19] Y. Gu and D. Zhang, "Interleaved boost converter with ripple cancellation network," *IEEE Transactions on Power Electronics*, vol. 28, no. 8, pp. 3860–3869, 2013, doi: 10.1109/TPEL.2012.2228505.

[20] B. B. Tuvar and M. H. Ayalani, "Analysis of a modified interleaved non-isolated cuk converter with wide range of load variation and reduced ripple content," *Proceedings of the International Conference on Trends in Electronics and Informatics, ICOEI 2019*, pp. 406–411, 2019, doi: 10.1109/ICOEI.2019.8862665.

[21] A. Dahono., A. Rizqiawan., and P. A. Dahono, "A modified Cuk DC-DC converter for DC microgrid systems," *Telkomnika (Telecommunication Computing Electronics and Control)*, vol. 18, no. 6, pp. 3247–3257, 2020, doi: 10.12928/TELKOMNIKA.v18i6.16466.

[22] P. A. Dahono, S. Riyadi, A. Mudawari, and Y. Haroen, "Output ripple analysis of multiphase dc-dc converters," *Proceedings of the International Conference on Power Electronics and Drive Systems*, vol. 2, pp. 626–631, 1999, doi: 10.1109/peds.1999.792732.

[23] M. N. A. Rabbani, A. Dahono, A. Rizqiawan, and P. A. Dahono, "A new family of bidirectional DC-DC power converters with very low input and output ripples," *Telkomnika (Telecommunication Computing Electronics and Control)*, vol. 20, no. 4, pp. 933–944, 2022, doi: 10.12928/TELKOMNIKA.v20i4.24215.

[24] X. Chen, D. Xu, F. Liu, and J. Zhang, "A novel inverter-output passive filter for reducing both differential- and common-mode dv/dt at the motor terminals in PWM drive systems," *IEEE Transactions on Industrial Electronics*, vol. 54, no. 1, pp. 419–426, 2007, doi: 10.1109/TIE.2006.885517.

[25] S. Du, B. Wu, K. Tian, D. Xu, and N. R. Zargari, "A Novel Medium-Voltage Modular Multilevel DC-DC Converter," *IEEE Transactions on Industrial Electronics*, vol. 63, no. 12, pp. 7939–7949, 2016, doi: 10.1109/TIE.2016.2542130.

BIOGRAPHIES OF AUTHORS

Nabil Driantama was born in Jakarta, Indonesia, in 1998. He received the bachelor education degree in electronical engineering education from the Universitas Negeri Jakarta, Jakarta, Indonesia, in 2020. His fields of research are power electronics and power system. At present, he is a graduate student at the Institute of Technology Bandung, Indonesia. He can be contacted at email: nabil23195@gmail.com.

Andriazis Dahono was born in Bandung, Indonesia, in 1994. He received the bachelor engineering degree in electrical engineering from the Institut Teknologi Sepuluh Nopember, Surabaya, Indonesia, in 2018. His fields of research are power electronics and power system. He is a recipient of the Korea Midland Power Company Scholarships. At present, he is a graduate student at the Institute of Technology Bandung, Indonesia. He can be contacted at email: andriazisd23@gmail.com.

Arwindra Rizqiawan was born in Salatiga, Indonesia. He received his bachelor and master's degree from Insititut Teknologi Bandung, Indonesia, in 2006 and 2008, respectively, and doctoral degree from Shibaura Insitute of Technology, Japan, in 2012, all in the field of electrical engineering. His current main interests are power engineering, power electronics, and renewable energy. He is currently serving as assistant professor in School of Electrical Engineering and Informatics, Institut Teknologi Bandung, Indonesia. He is certified professional engineer (IPM) in Indonesia by the Institution of Engineers Indonesia (PII), and ASEAN Engineer by ASEAN Engineering Register. He can be contacted at email: windra@itb.ac.id.

Jihad Furqani was born in Malang, East Java, Indonesia in 1990. He received a B.S. degree in electrical power engineering from Bandung Institute of Technology in 2012. He received an M.S. degree in electrical engineering from Bandung Institute of Technology in 2013. He received Dr. Eng degree in electrical and electronic engineering from Tokyo Institute of Technology in 2019. He has been studying multilevel and multiphase motor drives, noise reduction in switched reluctance motors, power electronic converters for renewable energy applications, and electric motors for vehicle applications. He was visiting researcher at the University of Akron in 2017 and visiting lecturer at the Tokyo Institute of Technology in 2021. Currently, he is a research assistant professor in Electrical Power Engineering, School of Electrical Engineering and Informatics, National Center for Sustainable Transportation Technology, and Center for Instrument Technology and Automation, Bandung Institute of Technology. He received IEEE Star Reviewer in 2019 and IEEE Indonesia Section Recognition in 2022. He can be contacted at email: jfurqani@itb.ac.id.